Amplitude Recovery and Deconvolution of Chirp and Boomer Data for Marine Geology and Offshore Engineering

Eleonora Denich [1,2] [iD], Aldo Vesnaver [2,*] [iD] and Luca Baradello [2] [iD]

[1] Department of Mathematics and Geosciences, University of Trieste, 34127 Trieste, Italy; edenich@inogs.it
[2] National Institute of Oceanography and Applied Geophysics-OGS, 34010 Sgonico, Italy; lbaradello@inogs.it
*   Correspondence: avesnaver@inogs.it

Abstract: The processing of Chirp data is limited by the usual recording of the signal envelope, which enhances its immediate visibility but prevents applying methods based on wave equations. This is normally not the case for Boomer data. However, both systems are monochannel instruments, which cannot estimate properly the propagation velocity of the signal in the rocks. In this paper, we present two theorems: the first one links the Chirp or Boomer source spectrum with an expected amplitude decay curve; the second one defines conditions for the deconvolution stability of the enveloped Boomer signal when the full waveform of the source signal is known. In this way, we can jointly process and integrate heterogeneous surveys including both data types. We validated the proposed algorithms by applying them to synthetic and real data. The presented tools can improve the image resolution and the characterization of geological formations in marine surveys by reflectivity anomalies, which are distorted by standard equalization methods.

Keywords: Chirp; Boomer; deconvolution; marine survey; sea floor characterization; envelope; gain recovery; inversion; offshore engineering

1. Introduction

The characterization of the sea floor properties and high-resolution images of the shallow geological formations just below the sea floor are very relevant for offshore engineering. Foundations of platforms for oil and gas productions must avoid shallow gas deposits, which may collapse under their huge weight [1]. In contrast, muddy or unconsolidated soils are preferable when it comes to deploying underwater communication cables, so they can be easily covered and better protected from interference by fish and humans [2]. Further applications include offshore engineering [3] and control of coastal erosion [4] and gas plumes' emission [5].

One of the expeditious geophysical methods for investigating the uppermost layer of the marine Holocenic sedimentary sequence in unconsolidated or poorly consolidated deposits is Chirp [6]. This very-high-resolution system is successfully applied to study the geologic framework of the inner-continental shelf [7], to solve geohazard [8] and environmental problems [9,10], to evaluate locations for the laying of pipelines [11], and for detection of marine archaeological sites [10,12]. Furthermore, [13] used Chirp to estimate the attenuation coefficients of sediments in Narragansett Bay and many authors studied techniques to classify the sediments with Chirp [14–16].

Chirp profiling systems are monochannel devices that emit an acoustic signal into sea water and record the echoes reflected back from the sea floor and the underlying shallow geological interfaces. The source and receiver use the same piezo-electric sensor array, whose frequency band usually ranges from 2 to 7 kHz. The signal waveform is composed of many adjacent peaks, so it is difficult to visually distinguish two signals with close travel times. For this reason, the signals' envelope is normally recorded and displayed. However, ref. [17] showed that recording and processing the original full waveform of the Chirp signal allows for exploitation of the monumental toolbox developed for seismic

data based on wave equations (as migration) or properties of the seismic signals (as the minimum phase of impulsive sources). The subsequent imaging improvements spectacular, as random noise and diffractions can be reduced significantly, allowing for a much better interpretation of the Chirp profiles.

The Chirp signal is obtained by a sweep, i.e., a set of frequencies emitted for a time span (normally, 10–20 ms) that are collapsed into a very short waveform by the cross-correlation of the emitted signal with the one back scattered from the sea floor and the underlying reflectors. Because of this genesis, the signal is symmetric in time, i.e., in geophysical jargon it is zero-phase. An alternative system is Boomer [18], whose signal is just a short pulse. Typical frequency bands for Boomer systems range from 400 to 9000 Hz [19]. As these bands are lower than those of Chirp data, Boomer surveys achieve a lower resolution but a higher penetration under the sea floor.

When taking the envelope of the original full-waveform data (either Chirp or Boomer) we lose some information, such as the signal polarity [5]. Some visual help for seismic interpreters, who are used to a bipolar signal, can be obtained by converting the positive-only enveloped signal into a seismic-like wavelet [20], which is better handled by conventional processing tools developed for seismic data. Still, when doing this kind of data assimilation, we must remember that the obtained reflectivity image may be correct for the signals' strength but not for their polarity.

In this paper, we present two theorems that allow for processing of enveloped Chirp or Boomer data without heavy assumptions or personal bias. First, we introduce a formula linking the amplitude decay in time of the signals to the source amplitude spectrum when propagating in a 3D anelastic medium. We show that this formula fits nicely the enveloped Chirp or Boomer data. Second, we present a theorem proving that the envelope of minimum-phase signals is also a minimum-phase signal. Thus, we can apply the same deconvolution methods developed for the usual seismic signals for the enveloped Boomer data based on the convolutional model of Earth's reflectivity. Using these tools, we can assimilate Chirp and Boomer data to process them jointly.

2. Amplitude Recovery

In the first two sections, we summarize the reasons for compensating the amplitude decay of a signal propagating in a 3D Earth model by a cumulative factor of t^2, where t is the propagation time, under tight simplifying assumptions [21]. In the third section, we present a more accurate gain curve that fits the spectral properties of the signal.

2.1. Geometrical Spreading

Chirp or Boomer sources emit an acoustic signal that propagates in the sea water and is scattered back by the sea floor and shallow acoustic reflectors. The sea water approximates well an elastic isotropic medium, and by approximating the source by a point, the signal propagates with spherical wavefronts in 3D. The total energy is preserved in time, but it is distributed over a surface whose extension is $4\pi r^2$, where $r = r(t)$ is the wavefront radius, i.e., the distance of the wavefront from the source point at a given time t. If the medium is homogeneous, $r(t) = v_p t$, where v_p is the P-wave velocity.

The frequency band of both Chirp and Boomer signals is quite wide, so that they approximate a spike in the time domain. If the signal is an ideal impulse with a white spectrum and amplitude $a(t)$, the total energy $E(t_0)$ at time t_0 is the integral of its squared amplitude over the wavefront with a radius r_0:

$$\mathrm{E}(t_0) = \oint_{W_1} a(t_0)^2 \, dS = 4\pi r_0^2 \, a(t_0)^2 \tag{1}$$

As the energy is constant during the propagation, for any other time t and corresponding radius r we must have:

$$E(t) = E(t_0) = 4\pi r^2 \, a(t)^2 \tag{2}$$

By rearranging and taking the square root, we obtain:

$$a(t) = \sqrt{\frac{E(t0)}{4\pi}}/r(t) = \sqrt{\frac{E(t0)}{4\pi}} \, (v_p t)^{-1} \tag{3}$$

Thus, there is an amplitude decay factor t^{-1} due to the geometrical spreading in a 3D homogeneous elastic medium.

2.2. Anelastic Absorption

While anelastic absorption is negligible in the sea water, it is not so in the marine sediments. The amplitude decay due to the anelastic absorption is frequency dependent. It is described by an exponential function $\exp(-\alpha \, \omega \, t)$, where ω is the angular frequency and α is the anelastic absorption coefficient; α depends on the lithology of the sediments. If we assume that the source spectrum is white and integrate this exponential function over all frequencies, we get:

$$\int_0^\infty e^{-\alpha\omega t}d\omega = \left[(-\alpha t)^{-1} e^{-\alpha\omega t}\right]_{\omega=0}^{\omega=\infty} = (\alpha t)^{-1} \tag{4}$$

which holds if $\alpha\omega > 0$. Therefore, allowing for anelastic absorption requires compensation for the amplitude decay for a further factor t^{-1} in addition to that due to the geometrical spreading.

2.3. Spectrum-Dependent Amplitude Recovery

The assumption of a white spectrum for the propagating signal is strong, and to attenuate it [21] discussed a more realistic case where the source spectrum can be approximated by the function $|\omega|^\beta$, where β is a data-dependent real parameter. This case is a bit unusual for seismic records, but it fits nicely with Chirp or Boomer enveloped data. Under this assumption, the comprehensive compensation function is suggested to be $t^{2+\beta}$, but the proof is left to the reader; we performed this exercise.

First of all, as the integral is to be taken over by all frequencies from zero to infinity, we can replace $|\omega|^\beta$ with just ω^β and then, using the integral formula 3.381 n.4 by [22], we get:

$$\int_0^\infty \omega^\beta e^{-\alpha t\omega}d\omega = \frac{1}{(\alpha t)^{\beta+1}}\Gamma(\beta+1)\,, \tag{5}$$

which holds if $\beta > -1$ and $\alpha > 0$, and where $\Gamma(\cdot)$ is the Gamma function. The resulting curve depends both on the anelastic absorption of the medium (via α) and on the source spectrum (via β). The latter can be estimated directly from the data, while the α parameter requires calibration values from rock physics and core analysis.

Figure 1 shows the full-waveform signal recorded by a real Chirp system and the corresponding envelope. The frequency range is 2–7 kHz. We notice the peaks complexity in the original data and the simpler shape of its envelope. Figure 2 shows the normalized amplitude spectrum of the original signal and that of its envelope (blue continuous curves). The superimposed orange dotted curve is the least-squares fit of a function $|\omega|^\beta$, where the optimal values for β were found to be, respectively, -0.278 and -0.545, using a least square fit. We can appreciate visually that a better fit was obtained for the envelope: its average absolute difference with the spectra was 0.0004 versus a value of 0.0360 for the original data. The envelope spectrum includes very low frequencies up to zero, unlike the original data.
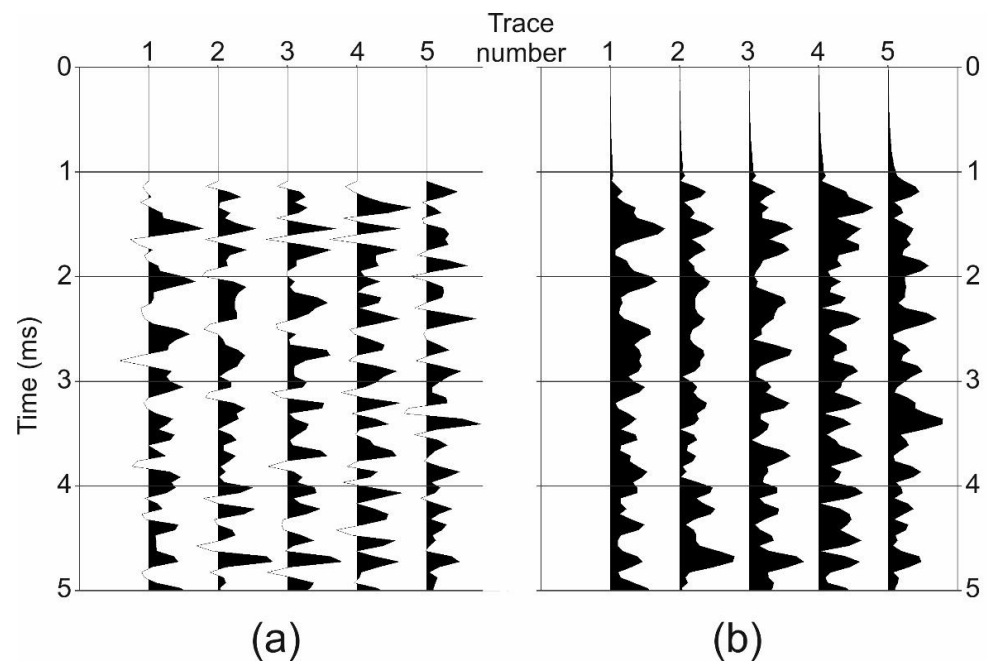
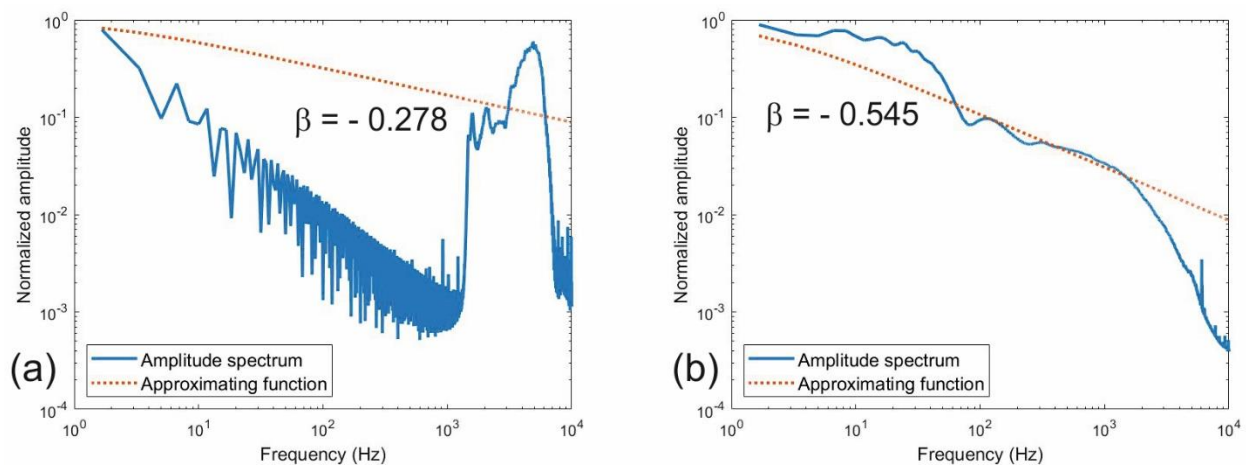**Figure 1.** Chirp data before (**a**) and after the envelope operator (**b**).

Figure 2. Normalized amplitude spectra of Chirp data before (**a**) and after (**b**) the envelope operator (continuous blue lines) plotted in a logarithmic scale. The approximating function $|\omega|^\beta$ is represented by the dotted orange line. Notice the different values in the two cases and the closer match for the enveloped Chirp data (**b**).

After compensation for the amplitude decay, the Chirp and Boomer seismograms are better able to approximate the key condition for a later processing step, i.e., the predictive deconvolution. This algorithm assumes that the received seismogram is the convolution of a (quasi)-stationary waveform with a random Earth reflectivity, whose amplitude spectrum should be (quasi)-white. In the next section, we consolidate the theoretical basis of this method when it comes to Boomer data.

3. Deconvolution

Offshore engineering involves construction in shallow waters, i.e., a few dozen meters. In this case, the reverberations between the sea surface and the bottom may obscure signals whose arrival time exceeds that from the first sea floor reflection. A satisfying solution exists for impulsive seismic data, i.e., a gapped deconvolution with prediction distance equal to the arrival time of the sea floor reflection [23]. As a special case, a spiking deconvolution (with a unit prediction distance) can enhance the resolution of the survey,

ideally collapsing the signal waveform into a spike. A key assumption for this method to work is the minimum-phase property of the signal, which guarantees that its inverse filter is stable. This property is well approximated by seismic signals produced by impulsive sources such as air guns, dynamite, and Boomer systems. Practical experience shows that deconvolution also works when enveloped Chirp data are processed [5]. The following theorem proves that enveloped Boomer data, whose original waveform is in a minimum phase, can be deconvolved to obtain stable results.

3.1. Deconvolution of Enveloped Minimum-Phase Signals

Theorem 1. *The envelope of a minimum-phase signal is still a minimum-phase signal.*

In order to prove this result, we need some preliminary considerations.
Let $r(t)$ be a real-valued seismic trace and $c(t)$ the related complex trace, such that

$$c(t) = r(t) + ir'(t), \tag{6}$$

where $r'(t) = H\{r(t)\}$ is the Hilbert transform of $r(t)$ and i is the imaginary unit. The envelope $e(t)$ is the modulus of the complex trace and is defined as

$$e(t) = |c(t)| = \left[r(t)^2 + r'(t)^2\right]^{\frac{1}{2}} \tag{7}$$

In discrete form, $r(t)$, $c(t)$, and $e(t)$ are given by the following sequences of observations, respectively:

$$(r_0, r_1, \ldots, r_m), \tag{8}$$

$$(c_0, c_1, \ldots, c_m), \tag{9}$$

$$(|c|_0, |c|_1, \ldots, |c|_m). \tag{10}$$

Let $P(z)$, $C(z)$, and $E(z)$ be the complex polynomials:

$$P(z) = r_0 + r_1 z + \ldots + r_m z^m, \tag{11}$$

$$C(z) = c_0 + c_1 z + \ldots + c_m z^m, \tag{12}$$

$$E(z) = |c|_0 + |c|_1 z + \ldots + |c|_m z^m, \tag{13}$$

which represent the Z-transforms of the sequences (8), (9), and (10), respectively. Assuming that all the zeros of $P(z)$ have a modulus greater than one, we want to show that the same holds true for the polynomial $E(z)$. By using the definition of the discrete Hilbert transform and the properties of the convolution, we can write the n-component c_n of sequence (9) as:

$$c_n = r_n + i(r * s)_n = (r * \delta)_n + i(r * s)_n = [r * (\delta + is)]_n, \tag{14}$$

where:

$$s_n = \begin{cases} 0, & | \text{ for } n \text{ even} \\ \frac{2}{\pi n}, & | \text{ for } n \text{ odd} \end{cases} \tag{15}$$

is an infinite impulse response, and

$$\delta_n = \begin{cases} 1, & | \text{ for } n = 0 \\ 0, & | \text{ for } n \neq 0 \end{cases} \tag{16}$$

is the Dirac delta function. From (14) and since the convolution in the time domain corresponds to multiplication in the z-domain, we have

$$C(z) = P(z)S(z) = c_0 + c_1 z + \ldots + c_m z^m, \tag{17}$$

with

$$S(z) = 1 + i\frac{2}{\pi} \sum_{j=0}^{\infty} \frac{z^{2j+1}}{2j+1} \,. \tag{18}$$

For the function $S(z)$ the following proposition holds true.

Proposition 1. *The root z_i of $S(z)$ are such that $|z_i| \geq 1$.*

Proof. Let us assume that $|z_i| < 1$. Since, for $|z| < 1$

$$\sum_{j=0}^{\infty} \frac{z^{2j+1}}{2j+1} = tanh^{-1}(z) \,, \tag{19}$$

then we should have:

$$1 + i\frac{2}{\pi}tanh^{-1}(z_i) = 0 \,. \tag{20}$$

The solution of (20) is:

$$z_i = tanh\left(\frac{\pi}{2}i\right) = -i\,tan\left(-\frac{\pi}{2}\right) \tag{21}$$

which shows the contradiction because $tan\left(-\frac{\pi}{2}\right) = -\infty$. $\square$

Now we can prove the Theorem.

Proof. By the Proposition, Equation (5), and by the assumption that the zeros of $P(z)$ have moduli greater than one, we have that $C(z)$ has all its roots with moduli greater than one. From Robinson [23], this is equivalent to saying that the series

$$\sum_{i=0}^{\infty} |c_i| \tag{22}$$

converges. Since the series (22) is the one associated to the polynomial $E(z)$, we can conclude that the zeros of $E(z)$ have moduli greater than one. $\square$

As a consequence of this theorem, the deconvolution of enveloped Boomer data will produce stable results, and its signal waveform can be compressed by a spiking deconvolution to increase the profile resolution.

3.2. Deconvolution of General Complex Signals

The Chirp signal is a symmetric, zero-phase waveform, and so is its envelope. Thus, the above theorem does not apply to this other type of data. We can design a shaping filter ([24,25], among many others) that converts this waveform into a minimum-phase one and then deconvolves the resulting traces. [20] showed that satisfying results can be achieved when the envelope data is transformed to a pseudo-seismic section. However, we must remark that the envelope operator causes a non-recoverable information loss when it comes to signal polarity.

After a compensation of the amplitude decay, we may approximate the Chirp or Boomer traces by the classical convolutional model. The real trace $r(t)$ is assumed to be the convolution of the real-valued sequence $x(t)$ of the Earth reflectivity with a signal wavelet $w(t)$:

$$r(t) = x(t) * w(t) \tag{23}$$

Taking the Hilbert transform of both sides, we obtain:

$$H\{r(t)\} = H\{x(t) * w(t)\} = x(t) * H\{w(t)\} = x(t) * w'(t) \tag{24}$$

where the prime sign stands for a Hilbert operator. Using (23) and (24), the complex trace $c(t)$ in (6) can be expanded as:

$$c(t) = x(t) * [w(t) + \mathrm{i}\, w'(t)] \tag{25}$$

We saw in the Theorem 1 that the Hilbert operator preserves the minimum phase of the sequence it is applied to. Thus, if $w(t)$ is a minimum phase, so too is $w'(t)$, and we may also apply the deconvolution algorithms designed for real-valued traces to complex traces.

4. Application to Real Geophysical Data

To validate the presented algorithms for amplitude recovery and deconvolution, we applied them to two profiles acquired by the OGS, the Italian National Institute of Oceanography and Applied Geophysics in the Gulf of Trieste (Adriatic Sea): a Chirp profile acquired by the OGS-Explora vessel in shallow waters and an intersecting Boomer profile acquired by a smaller boat described below. The shallow waters (about 15–20 m) cause major reverberations, which are usually attenuated by a gapped deconvolution in seismic processing.

The Chirp survey was carried out using a system Benthos CAP-6600 Chirp II Data-Sonics, with an array of 16 receivers hull-mounted on board at a depth of 4.32 m. The frequency band ranged from 2 to 7 kHz. The sampling interval was 0.132 ms and the shooting frequency was 2 times per second. The Boomer survey was carried out with an electro-dynamic transducer UWAK Nordik Nord mounted on a catamaran frame that suspends the source at a constant depth of 40 cm to avoid dragging turbulence. The seismograms were acquired using a pre-amplified oil-filled mono-channel streamer composed of eight piezoelectric elements, for a total active section of 2.8 m. The source and the receiver were towed with parallel geometry to minimize the normal move-out correction that is needed to compensate for the source–receiver offset [26].

Figure 3 shows a Chirp profile without any gain recovery (Figure 3a) and using an automatic gain control (AGC) with two different window lengths: a mild one with 10 ms (Figure 3b) and a stronger one with 3 ms (Figure 3c). Both AGC results were poor: the longer window introduced blanked areas around the sea floor reflection at 25–26 ms and its multiples at 50–52 and 75–78 ms; the shorter window reduced the blanking but emphasized the random noise and the multiple reverberations.
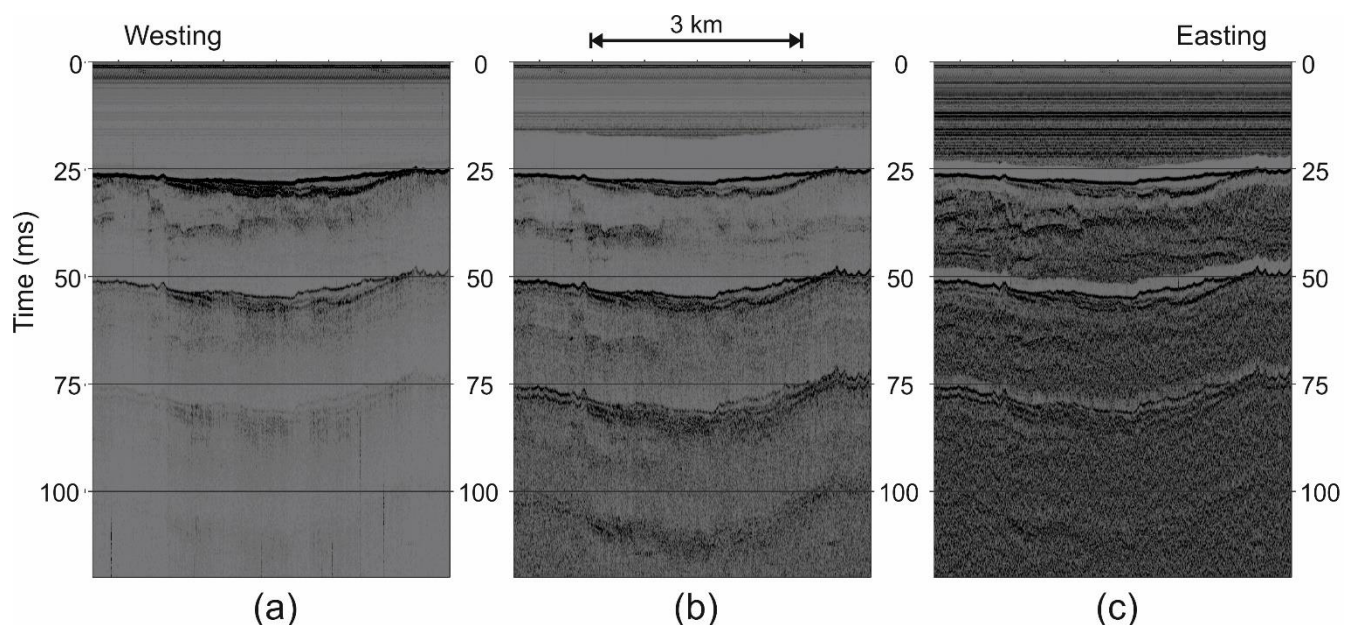

Figure 3. Chirp data without gain recovery (**a**) and with an automatic gain control using a window length of 10 ms (**b**) and 3 ms (**c**).

When applying a gain curve t^α, i.e., with an exponent α of the arrival time t (Figure 4), the sections look much better. First of all, the direct arrivals and the sea water layers are visible, although no mute was applied, because of the overwhelming amplitude of the sea floor reflection. For $\alpha = 1$ (Figure 4a), we compensated only for the geometrical spreading, neglecting the anelastic absorption of the sediments. This is a good approximation for the water reverberations but not for the propagation below the sea floor. For $\alpha = 2$ (Figure 4c), we assume that both sea water and sediments introduce some frequency loss and that the source spectrum is white. This results in an overcorrection of the signal amplitude for long travel times. An intermediate result is obtained for $\alpha = 1.473$ (Figure 4b), a value computed using the spectral fit discussed above. Visually, it looks reasonable, but more reasons are needed for preferring it to the other results obtained so far.
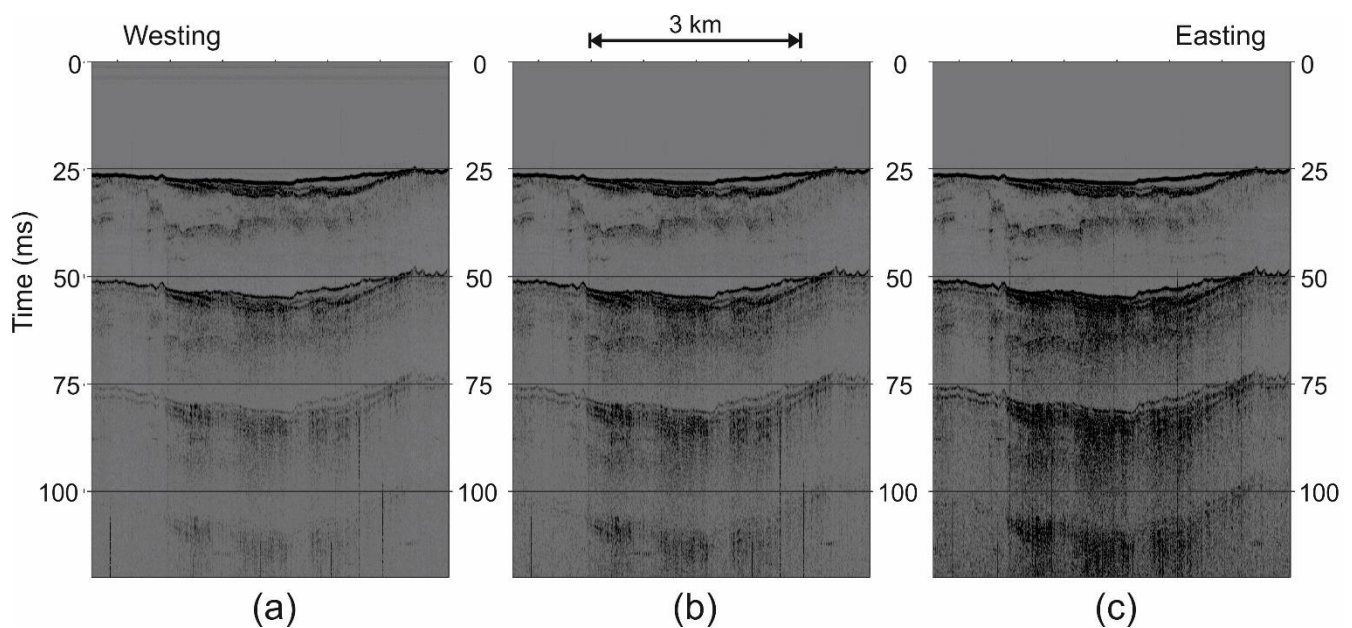

Figure 4. The same data as in Figure 3 using three different a exponent values for the gain curve t^α: $\alpha = 1$ (**a**), $\alpha = 2 + \beta = 2 - 0.527 = 1.473$ (**b**), and $\alpha = 2$ (**c**).

Figure 5 shows the effects of a gapped deconvolution with a prediction distance of 23 ms applied to the same data as in Figure 4. The multiple attenuation is remarkably good when applied to the traces corrected by $\alpha = 1$ (Figure 5a), a bit poorer for $\alpha = 1.473$ (Figure 5b), and definitely worse for $\alpha = 2$ (Figure 5c). This result is explained by the optimal stationarity achieved by the reverberated signals when compensating only for the spherical divergence and assuming no anelastic absorption in the water. As mentioned above, this is a good approximation. Again, $\alpha = 2$ is poor, and $\alpha = 1.472$ is just fair. However, any result based on a t^α curve is far better than those obtained using an AGC (Figure 6), whether with a long window (Figure 6b) or a short one (Figure 6c). In both cases, the multiple attenuation is minimal and the image quality very questionable. An interesting solution is obtained in two steps (Figure 6a): after a gain recovery with $\alpha = 1$ and a gapped deconvolution (Figure 5a), we applied a further gain curve that was recalculated for the deconvolved data based on its (now modified) spectral properties. The fit result for the β correction was -0.485, which is lower than that of -0.527 for the original data. For a perfectly elastic medium and a white-spectrum source, the ideal value would be -1, while for a strongly absorbing medium it would approximate 0. Thus, the value for the two-step deconvolution, closer to zero, is consistent with the expected higher absorption in the shallow sediments. These values are averages along the profile; the possible quantitative use of this parameter for local analysis is an interesting research topic for future studies. From a practical point of view, however, we cannot claim that this two-step procedure provides major advantages; the differences between Figures 5a and 6a are barely visible.
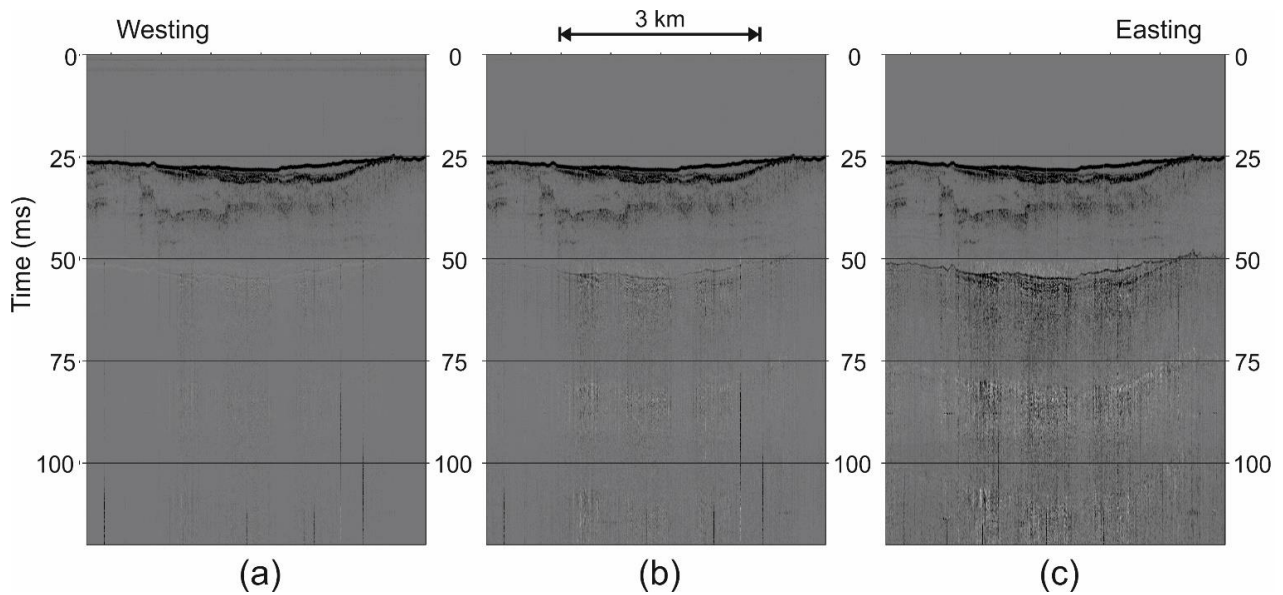
Figure 5. Gapped deconvolution for the same data as in Figure 4, i.e., using α exponents: $\alpha = 1$ (**a**), $\alpha = 1.473$ (**b**), and $\alpha = 2$ (**c**). The best result in terms of multiple attenuation is obtain for $\alpha = 1$ (**a**), as the sea water approximates well a perfectly elastic medium.
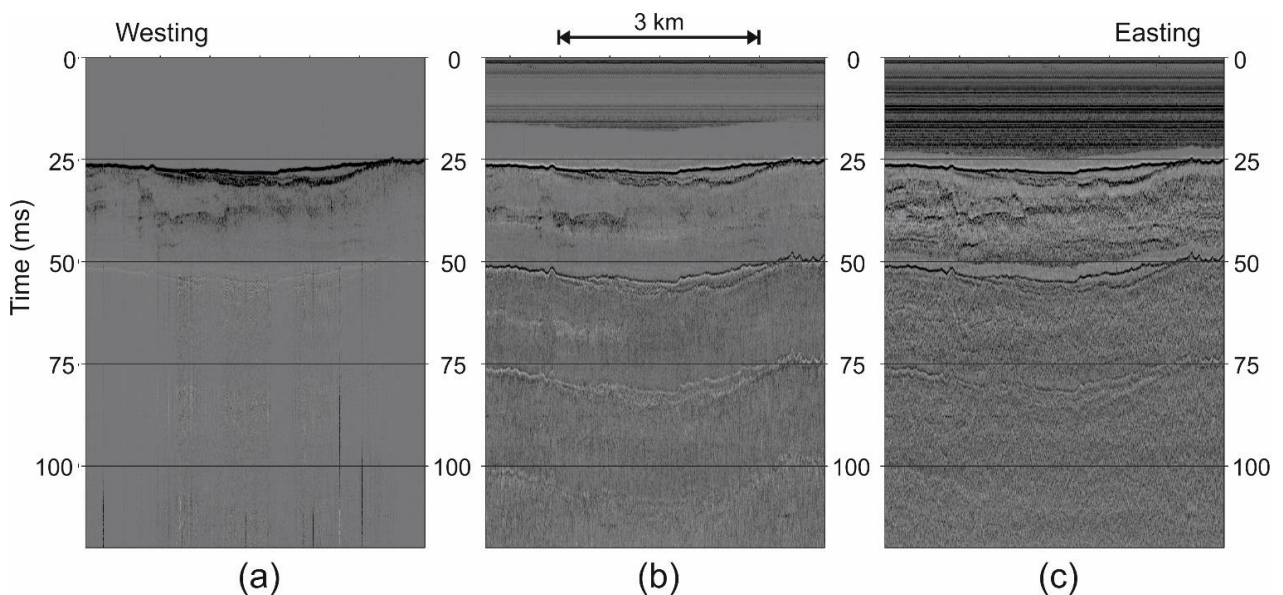

Figure 6. Gapped deconvolution applied in two steps (**a**) and after the AGC using the two windows as in Figure 3, i.e., 10 ms (**b**) and 3 ms (**c**). After AGC, the multiples' residuals are much stronger than those obtained using any t^{α} gain curve (Figure 5).

Figure 7 shows the two alternate processing strategies. One option is applying a cumulative gain curve in one step only (right), so obtaining a kind of average compensation including multiples and primaries; the other option (left) is compensating for the spherical divergence first, so maximizing the multiples' stationarity in terms of signal amplitude, then applying a deconvolution, and finally compensating for the anelastic absorption, which affects mainly the primaries. The first option is simpler, the second seems more accurate, but their difference is tiny. An ideal way for choosing between them would be a calibration by well logs, as done routinely in the oil and gas industry for much deeper formations and much lower frequencies. Unfortunately, this additional data is almost never available for shallow marine surveys, so we must adopt physical solidity and visual interpretability as the criteria.
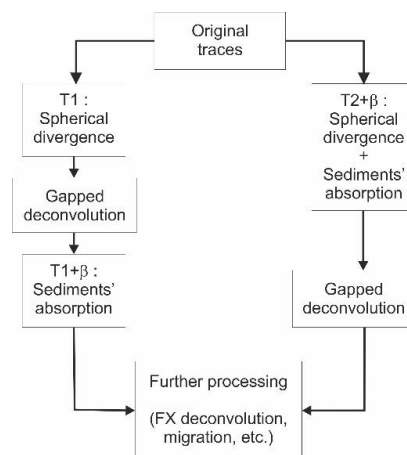
Figure 7. Two possible strategies for multiples' attenuation: one step only (right), when the deconvolution follows the full gain recovery; and two steps (left), when the deconvolution follows the spherical divergence correction, which enhances the multiples, but precedes the gain compensation for the absorption based on the spectrum shape of the seismic traces.

Figure 8 shows the location of two intersecting profiles acquired at the Gulf of Trieste (Adriatic Sea) and Figure 9 shows their spectral fit. Both are enveloped data: one acquired by the Chirp system and the other one by the Boomer system (Figure 10). Their β values are different: -0.558 for the Chirp data versus -0.645 for the Boomer data. Nevertheless, when applying the resulting $t^{2+\beta}$ function to each of them, we obtain well balanced images for the amplitude as a function of time (Figure 11). The Boomer data (Figure 11b) reveal intriguing primary signals, with arrival times at 75 and 110 ms, which are not visible in the Chirp section at all (Figure 11a). However, the irregular horizon between 50 and 55 ms is nicely enhanced when compared with that of the unprocessed data in Figure 10. Furthermore, the gain curve attenuates the direct arrivals or shallow scattering, between 0 and 15 ms, so that we do not need to apply a shallow mute to clean the sections in the water layer.
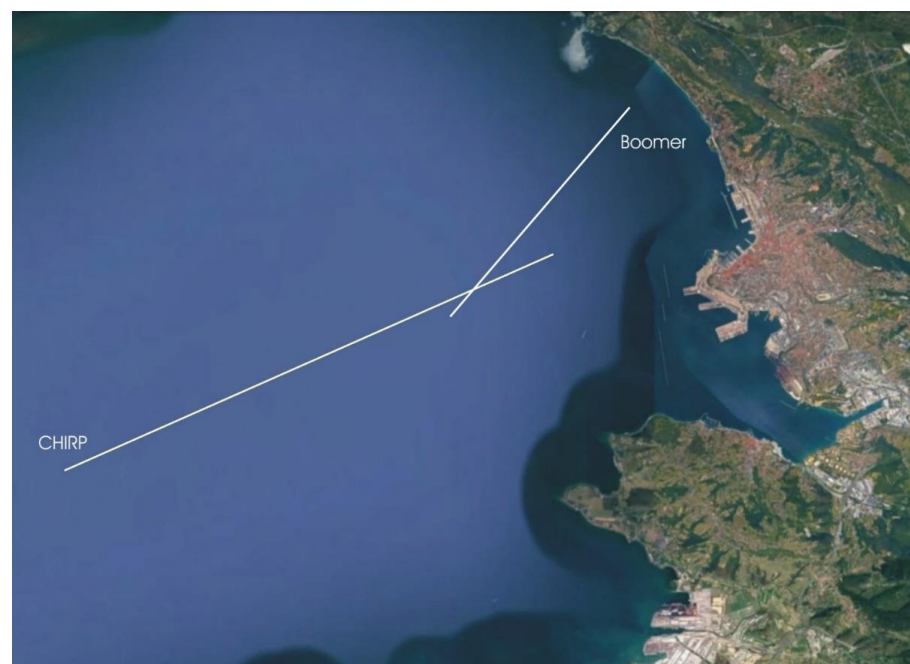

Figure 8. Location map of two intersecting profiles at the Gulf of Trieste (northern Adriatic Sea): one acquired by a Chirp system, the other with a Boomer system.
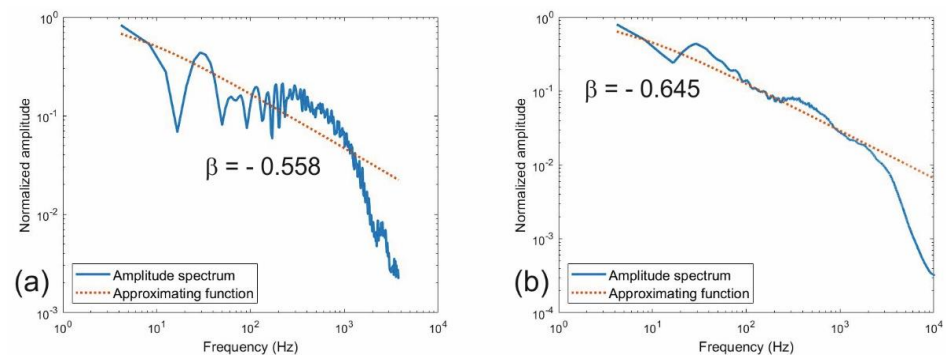
Figure 9. Normalized amplitude spectra for two intersecting profiles with enveloped Chirp (**a**) and enveloped Boomer data (**b**) plotted by continuous blue lines in a logarithmic scale. The approximating function $|\omega|^{\beta}$ is represented by the dotted orange line. Notice the different b values in the two cases, and the closer match of the enveloped Boomer data (**b**) to the approximating function.
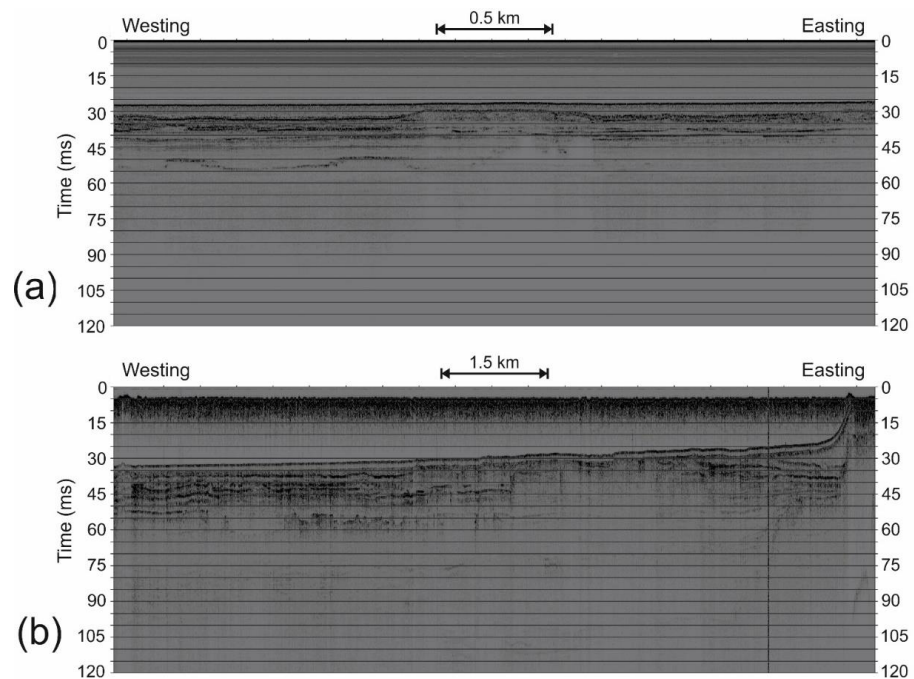

Figure 10. Two intersecting profiles acquired at the Gulf of Trieste (Adriatic Sea) using a Chirp system (**a**) and a Boomer system (**b**).

In Figure 11, we marked the intersection point of the two profiles by dotted lines. We notice that there is a mismatch of about 5 ms between the sea floor reflection of the Chirp data (at 28 ms) and that of the Boomer data (at 33 ms). The reason is the depth difference from the sea surface of the two systems: 4.3 m for the Chirp data and 0.3 m for the Boomer data. Assuming a P velocity for the sea water of 1500 m/s, this depth difference implies a two-way time delay of 5.3 ms, which fits nicely with what we observed. A further minor difference may also be due to different tide phases during the two surveys.

Figure 12 shows two composite sections of Chirp and Boomer data after a spiking deconvolution: first, plotting the left chunk of the Boomer data, up to the intersection point, and then the right chunk of the Chirp data (Figure 12a); then, the opposite with the two other parts (Figure 12b). The Boomer parts are noisier and contain lower frequencies, but they display clearer primary events between 50 and 60 ms. Along the intersection lines, the reflections are kinematically consistent, displaying a good lateral continuity. Thus, a consistent geological interpretation can be extended across the whole play, taking advantage of this and other intersections of the different recording campaigns.
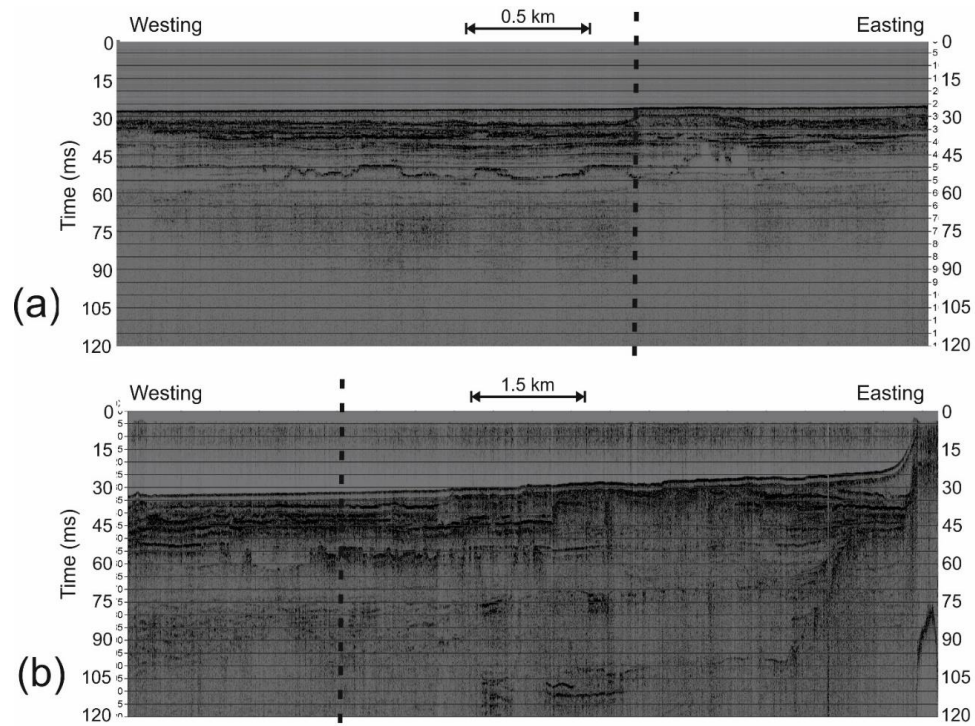
Figure 11. The two profiles in Figure 10 after a gain recovery using the β terms in Figure 9. The dotted vertical lines indicate the intersection points. The Boomer source (**b**) highlights deeper events than does the Chirp source (**a**).
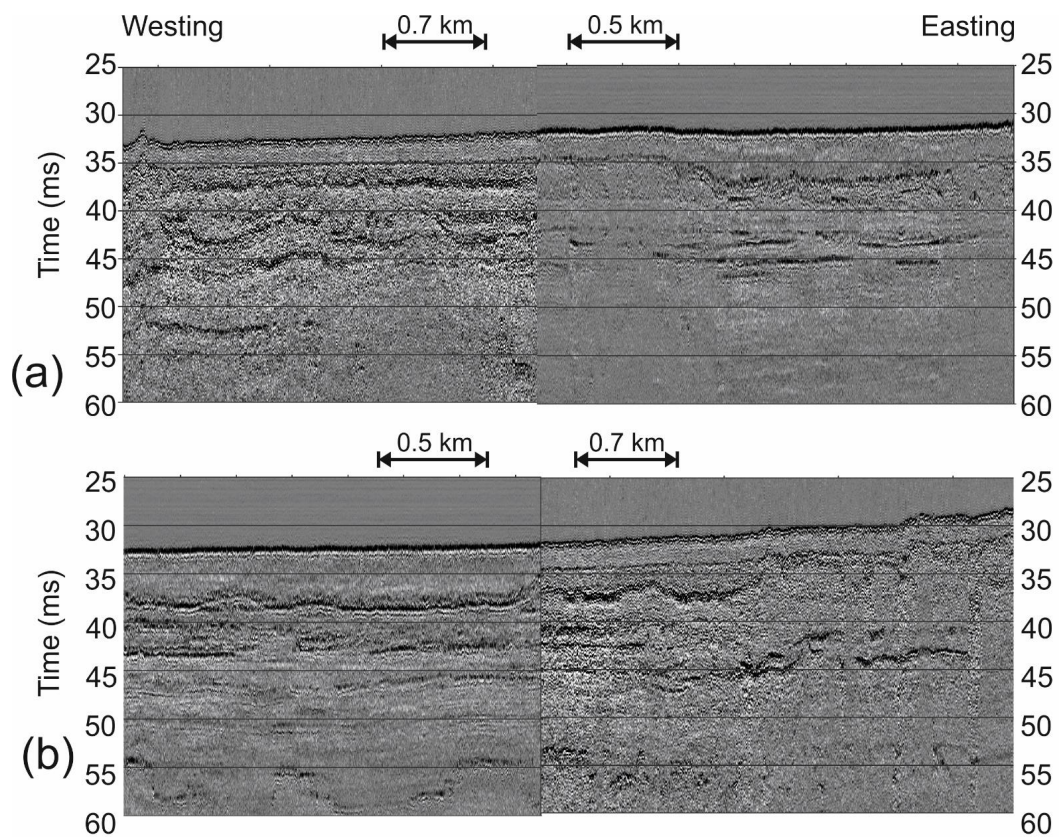

Figure 12. Details at the intersection point of the Boomer and Chirp profiles after a spike deconvolution: Boomer-Chirp (**a**) and Chirp-Boomer (**b**). The Boomer data are noisier, but their lower frequencies penetrate further than do the better-resolved Chirp data.

5. Conclusions

Processing of Chirp and Boomer data is limited by the monochannel acquisition systems, which prevent using the propagation velocity of waves to distinguish primary and multiple reflections. Nevertheless, a gapped deconvolution with a prediction distance equal to the distance to the sea floor is an effective tool for attenuating multiples. To work in optimal conditions, a compensation for the amplitude decay due to geometrical spreading and anelastic absorption is needed. In this paper, we provided the detailed formula envisaged by Claerbout (1985), which defines an effective gain curve based on the source spectrum. We found that this fit is particularly good when it comes to enveloped Chirp or Boomer data.

A theorem was presented stating that the envelope of a minimum-phase signal is still a minimum phase waveform. This allows for theoretically validating the use of deconvolution for enveloped data, in particular for the Boomer case, when deconvolving those data and comparing them with Chirp profiles. This possible workflow, although uncommon, allows for the merging of heterogeneous surveys with Chirp and Boomer data into a consistent play.

Author Contributions: E.D. demonstrated the Theorem and created the mathematical parts of the text; A.V. suggested the paper topic and created the geophysical parts of the text; L.B. provided the real data and undertook their basic processing. All authors contributed to the discussion, the conclusions, and the text revision. All authors have read and agreed to the published version of the manuscript.

Data Availability Statement: The Boomer data used in this paper may be obtained by request to Luca Baradello (lbaradello@inogs.it) and the Chirp data by request to Martina Busetti (mbusetti@inogs.it).

Conflicts of Interest: The authors declare no conflict of interest.

References

1. Gylland, A.S.; de Vries, M.H. The effect of gas blow-out on shallow offshore foundations. In Proceedings of the Second British Geotechnical Association International Conference on Foundations 2008, Dundee, UK, 24–27 June 2008; pp. 885–896, ISBN 9781848060449.
2. Yincan, Y.; Xinmin, J.; Guofu, P.; Wei, J. (Eds.) *Submarine Optical Cable Engineering, Chapter 5—Engineering Site Survey for Submarine Optical Cable*; Academic Press: Cambridge, MA, USA, 2018; ISBN 9780128134757. [CrossRef]
3. Masoli, C.A.; Petronio, L.; Gordini, E.; Deponte, M.; Boehm, G.; Cotterle, D.; Romeo, R.; Barbagallo, A.; Belletti, R.; Maffione, S.; et al. Near-shore geophysical and geotechnical investigations in support of the Trieste Marine Terminal extension. *Near Surf. Geophys.* **2019**, *18*, 73–89. [CrossRef]
4. De Souza, J.A.G.; Barletta, R.D.C.; Franklin, L.; Benedet, L. Utilization of multiple geophysical sources and geotechnical sampling to search for offshore sand deposits for beach restoration in Brazil. In *2015 IEEE/OES Acoustics in Underwater Geosciences Symposium (RIO Acoustics)*; IEEE: New York, NY, USA, 2015; pp. 1–4. [CrossRef]
5. Vesnaver, A.; Busetti, M.; Baradello, L. Chirp data processing for fluid flow detection at the Gulf of Trieste (northern Adriatic Sea). *Bull. Geophys. Oceanogr.* **2021**. [CrossRef]
6. Gutowski, M.; Bull, J.; Henstock, T.; Dix, J.; Hogarth, P.; Leighton, T.; White, P. Chirp sub-bottom profiler source signature design and field testing. *Mar. Geophys. Res.* **2002**, *23*, 481–492. [CrossRef]
7. Schwab, W.C.; Thieler, E.R.; Allen, J.R.; Foster, D.S.; Swift, B.A.; Denny, J.F. Influence of Inner-Continental Shelf Geo-logic Framework on the Evolution and Behavior of the Barrier-Island System between Fire Island Inlet and Shinnecock Inlet, Long Island, New York. *J. Coast. Res.* **2000**, *16*, 408–422. Available online: https://www.jstor.org/stable/4300050 (accessed on 9 September 2021).
8. Dyer, J.M. Geohazard identification: The gap between the possible and reality in geophysical surveys for the engineering industry. *Mar. Geophys. Res.* **2011**, *32*, 37–47. [CrossRef]

9. Ercilla, G.; Córdoba, D.; Gallart, J.; Gràcia, E.; Muñoz, J.A.; Somoza, L.; Vázquez, J.T.; Vilas, F. Geological characterization of the Prestige sinking area. *Mar. Pollut. Bull.* **2006**, *53*, 208–219. [CrossRef] [PubMed]
10. Grøn, O.; Boldreel, L.O. Chirping for Large-Scale Maritime Archaeological Survey: A Strategy Developed from a Practical Experience-Based Approach. *J. Archaeol.* **2014**, *2014*, 1–11. [CrossRef]
11. Tian, W.-M. Integrated method for the detection and location of underwater pipelines. *Appl. Acoust.* **2008**, *69*, 387–398. [CrossRef]
12. Plets, R.; Dix, J.; Adams, J.; Best, A. 3D reconstruction of a shallow archaeological site from high-resolution acoustic imagery: The Grace Dieu. *Appl. Acoust.* **2008**, *69*, 399–411. [CrossRef]
13. Schock, S.G.; Leblanc, L.R.; Mayer, L. Chirp subbottom profiler for quantitative sediment analysis. *Geophysics* **1989**, *54*, 445–450. [CrossRef]
14. Panda, S.; Leblanc, L.R.; Schock, S.G. Sediment classification based on impedance and attenuation estimation. *J. Acoust. Soc. Am.* **1994**, *96*, 3022. [CrossRef]
15. Stevenson, I.; McCann, C.; Runciman, P. An attenuation-based sediment classification technique using Chirp sub-bottom profiler data and laboratory acoustic analysis. *Mar. Geophys. Res.* **2002**, *23*, 277–298. [CrossRef]
16. Rui, W.; Li Changzheng, L.; Yan Xiaofei, X. Application of Sub-Bottom Profiler to Study Riverbed Structure and Sediment Density. *IOP Conf. Ser. Earth Environ. Sci.* **2018**, *128*, 012113. [CrossRef]
17. Baradello, L. An improved processing sequence for uncorrelated Chirp sonar data. *Mar. Geophys. Res.* **2014**, *35*, 337–344. [CrossRef]
18. Simpkin, P.G. The Boomer Sound Source as a Tool for Shallow Water Geophysical Exploration. *Mar. Geophys. Res.* **2005**, *26*, 171–181. [CrossRef]
19. Donda, F.; Brancolini, G.; Tosi, L.; Kovacevic, V.; Baradello, L.; Gačić, M.; Rizzetto, F. The ebb-tidal delta of the Venice Lagoon, Italy. *Holocene* **2008**, *18*, 267–278. [CrossRef]
20. Baradello, L.; Battaglia, F.; Vesnaver, A. Fast method to transform chirp envelope data into pseudo-seismic data. *Mar. Geophys. Res.* **2021**, *42*, 1–11. [CrossRef]
21. Claerbout, J. *Imaging the Earth's Interior*; Blackwell: Oxford, UK, 1985; pp. 233–234.
22. Gradshteyn, I.S.; Ryzhik, I.M. *Table of Integrals, Series, and Products*, 7th ed.; Jeffrey, A., Zwillinger, D., Eds.; Elsevier and Academic Press: Amsterdam, The Netherlands, 2007; p. 346.
23. Robinson, E.A. Predictive decomposition of time series with application to seismic exploration. *Geophysics* **1967**, *32*, 418–484. [CrossRef]
24. Claerbout, J. *Fundamentals of Geophysical Data Processing*; McGraw-Hill: New York, NY, USA, 1976; pp. 130–133.
25. Claerbout, J. *Earth Soundings Analysis: Processing Versus Inversion*; Blackwell: Oxford, UK, 1992; pp. 150–154.
26. Baradello, L.; Carcione, J.M. Optimal seismic-data acquisition in very shallow waters: Surveys in the Venice lagoon. *Geophysics* **2008**, *73*, Q59–Q63. [CrossRef]